Contrib Mineral Petrol (2003) 144: 703–721
DOI 10.1007/s00410-002-0424-z

ORIGINAL PAPER

Carl J. Spandler · Richard J. Arculus
Stephen M. Eggins · John A. Mavrogenes
Richard C. Price · Anthony J. Reay

Petrogenesis of the Greenhills Complex, Southland, New Zealand: magmatic differentiation and cumulate formation at the roots of a Permian island-arc volcano

Received: 3 January 2002 / Accepted: 23 September 2002 / Published online: 19 November 2002

Abstract A Permian (~265 Ma) intrusive complex which formed as a magmatic feeder reservoir to an immature island-arc volcano is fortuitously exposed in southern New Zealand. Known as the Greenhills Complex, this intrusion was emplaced at shallow crustal levels and consists of two layered bodies which were later intruded by a variety of dykes. Cumulates, which include dunite, olivine clinopyroxenite, olivine gabbro, and hornblende gabbro-norite, are related products of parent-magma fractionation. Both primary (magmatic) and secondary platinum-group minerals occur within dunite at one locality. Using the composition of cumulus minerals, mafic dykes and melt inclusions, we have determined that the parent magmas of the complex were hydrous, low-K island-arc tholeiites of ankaramitic affinities. Progressive magmatic differentiation of this parent magma generated fractionated melt of high-alumina basalt composition which is now preserved only as dykes which cut the Complex. Field evidence and cumulus mineral profiles reveal that the magma chambers experienced turbulent magmatic conditions during cumulate-rock formation. Recharge of the chambers by primitive magma is likely to have coincided with eruption of residual melt at the surface. Similar processes are inferred to account for volcanic-rock compositions in other parts of this arc terrane and in modern island-arc systems.

C.J. Spandler (✉) · R.J. Arculus · J.A. Mavrogenes
Department of Geology,
Australian National University, 0200 Canberra, Australia
E-mail: carl@geology.anu.edu.au
Tel.: +61-261252056
Fax: +61-261255544

S.M. Eggins · J.A. Mavrogenes
Research School of Earth Sciences,
Australian National University, 0200 Canberra, Australia

R.C. Price
School of Science and Technology,
University of Waikato, Hamilton, New Zealand

A.J. Reay
Geology Department, University of Otago,
Dunedin, New Zealand

Editorial responsibility: T.L. Grove

Introduction

Understanding of the geochemistry of island-arc systems has been determined mainly from studies of volcanic rocks from modern arc environments. It is now widely accepted that the majority of island-arc magmatism is generated by melting of a peridotitic mantle source which has previously been modified by subduction-related fluids and/or melts (Arculus and Powell 1986; Hawkesworth et al. 1993; Pearce and Peate 1995). However, most arc-related volcanic rocks have relatively evolved compositions which are not directly compatible with such a primitive mantle source (Perfit et al. 1980). This is generally argued to indicate that parental magmas undergo significant differentiation at the sub-volcanic level. The intrusive products of such fractionation processes are expected to comprise many times the volume of the extrusive rocks of a typical arc (Ito et al. 1983). Nonetheless, relatively little is known about the sub-volcanic environment of island arcs. Xenoliths from arc lavas provide some information on cumulates and magmas formed at depth, but well-preserved, primitive island-arc intrusives are rarely exposed.

The Greenhills Complex of South Island, New Zealand is a small intrusive body which was part of a Permian intra-oceanic arc system. The Complex consists of a variety of well-exposed and well-preserved cumulates and crosscutting dykes, and provides an excellent opportunity to study in detail the magmatic processes which occur in the early stages of high-Mg island-arc magmatism. Here, we outline the petrology, mineralogy and geochemistry of rocks of the Complex, describe their dynamic magmatic history and determine the geochemical evolution of the parental magmas during formation of the cumulates. This work has important

implications for magma genesis and evolution in arc environments, the nature of coexisting mineral assemblages, crystallisation sequences, and may contribute to a greater understanding of crustal growth.

Geological setting

The pre-Cainozoic geology of New Zealand consists largely of a series of unrelated tectono-stratigraphic terranes which were juxtaposed by the end of the Cretaceous (Coombs et al. 1976; Mortimer 1995). The Brook Street Terrane comprises a 14-km-thick sequence of Permian volcanic and volcaniclastic (basaltic to andesitic) rock which is now preserved as a north-south-trending linear belt which extends the length of the South Island (Bradshaw 1994). The southern portion of the terrane is shown in Fig. 1. Sedimentary and geochemical characteristics suggest terrane formation in an intra-oceanic arc setting (Sivell and Rankin 1983; Frost and Coombs 1989; Houghton and Landis 1989). Throughout the Brook Street Terrane, mafic to ultramafic intrusive complexes of Permian to Triassic age have been emplaced at shallow crustal levels. The Greenhills Complex is the largest and best exposed of these complexes.

The Greenhills Complex occupies a broad headland along the southern shoreline of the South Island, 15 km south of Invercargill (Fig. 1). It has intruded a sequence of island arc-derived sediments and tuffs known as the Greenhills Group (Mossman and Force 1969; Frost and Coombs 1989), causing a small (< 200 m) hornblende–hornfels contact aureole (Mossman 1973). The regional metamorphic grade is of prehnite-pumpellyite facies, constraining the emplacement depth to less than 10 km. The Complex consists of two layered intrusions (Northern and Southern) of similar character, which have a combined area of 14 km^2 (Fig. 2). These intrusions comprise a concentrically arranged sequence of ultramafic to mafic cumulate-rock types which we refer to as the Layered Group. Layered Group rock types of the Southern Intrusion include dunite, olivine clinopyroxenite, olivine gabbro and hornblende gabbro-norite. Exposures of the Northern Intrusion consist almost completely of olivine clinopyroxenite and olivine gabbro. Structural features are rarely found within the ultramafic rocks. However, ubiquitous layering in the gabbroic rocks consistently dips towards the core of the intrusion (Fig. 2), indicating that the gabbros stratigraphically overlie the ultramafic rocks. We interpret that both intrusions have funnel or bowl-like shapes.

Intruding the Layered Group are numerous dykes of varying composition and several smaller cumulate bodies. Field relations indicate that most of the dykes were emplaced soon after crystallisation of the cumulates. The most extensive of these is a gabbroic ring dyke which encloses the Layered Group and forms the outer margins of the Complex. Exposures of other dykes occur

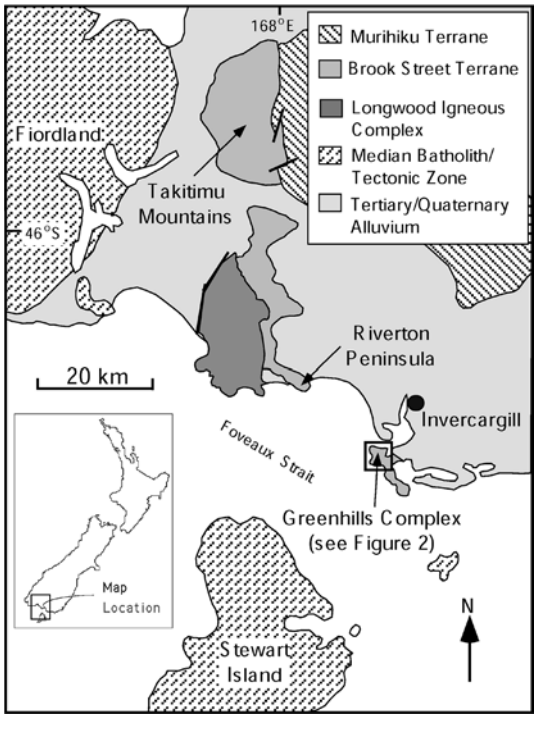

Fig. 1 Geologic units of southern New Zealand

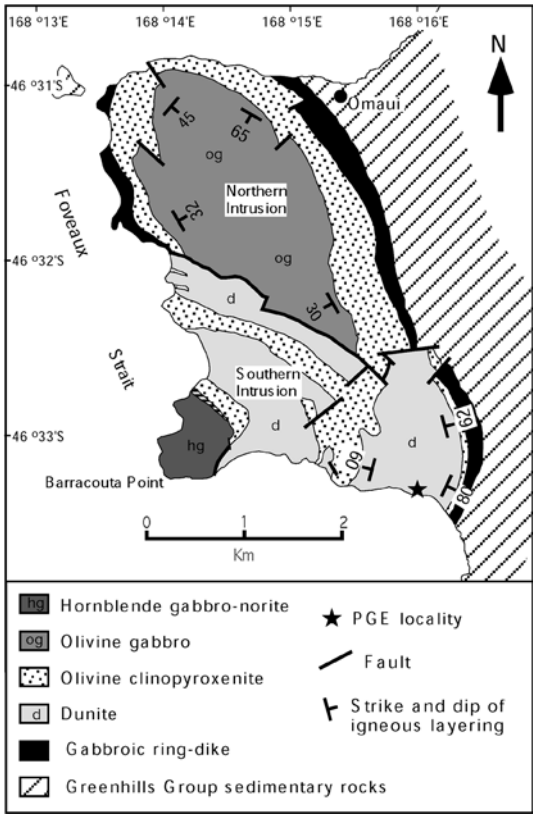

Fig. 2 Geology of the Greenhills Complex (modified from Spandler et al. 2000)

throughout the Complex but rarely exceed 100 m in length. Small (< 50 m in diameter) cumulate bodies of troctolite to magnetite gabbro-norite intrude the southern margin of the complex. These intrusions generally display spectacular rhythmic layering, but they clearly postdate the emplacement of the Layered Group and are not discussed further here.

Absolute age constraints for the Greenhills Complex are limited to a single U–Pb date of 265 Ma, obtained from a hornblende gabbro-norite sample (Kimbrough et al. 1992). A Sm–Nd date of 270 ± 5 Ma obtained for the Greenhills Group (Frost and Coombs 1989) is consistent with the early Permian age inferred from the abundant fossil evidence preserved in these sediments (Mossman and Force 1969). These dates indicate that the Greenhills Complex and the Greenhills Group sediments are of similar age and hence, are likely to be of related tectonic setting.

General geology of the Layered Group

Dunite

The dominant rock type of the Southern Intrusion is dunite which comprises two massive units, each up to 900 m in outcrop width (Fig. 2). By contrast, outcrops of dunite from the Northern Intrusion are restricted to a few small (< 5 m) blocks enclosed within olivine clinopyroxenite. Layering and other structures are largely absent from all dunite units, although well-developed cleavage has been observed in several outcrops. Olivine clinopyroxenite is the only rock type in original contact with dunite. Most of these contacts are gradational over a few centimetres, indicating that the transition between rock types formed from original cumulate processes. An exception is the brecciated and intermixed contacts (Fig. 3A) which occur in the Southern Intrusion where dunite overlies olivine clinopyroxenite.

Fig. 3 **A** Intermixed contact between olivine clinopyroxenite (*dark*) and dunite (*light*), Southern Intrusion. **B** Strongly folded block of interlayered olivine gabbro (*light*) and olivine clinopyroxenite (*dark*), Northern Intrusion. **C** Block of interlayered olivine gabbro (*light*) and olivine clinopyroxenite (*dark*) which has been brecciated, Northern Intrusion. Hammer handle length is approximately one metre

There is little variation in the proportions of original cumulus minerals in the dunites. These include forsteritic olivine, comprising 98–99% of the rock, and 1–2% interstitial chromian spinel. Clinopyroxene may be present in trace amounts. Original olivine grain size ranges from 1 to 3 mm whereas chromian spinels are generally less than 0.5 mm in size. Chromian spinels commonly contain small (< 50 μm) olivine, clinopyroxene and multiphase inclusions. The multiphase inclusions may contain olivine, clinopyroxene, spinel, amphibole and residual melt phases, and are interpreted to have been original melt which was trapped by the crystallising spinel grains (Spandler et al. 2000). All of the olivine is fractured and partially replaced by serpentine and magnetite, although where olivine is intensely altered, iddingsite, chlorite and magnetite dominate.

Randomly orientated chromian-spinel schlieren (1 cm to 1 m in length) occur within dunite in several places in the Southern Intrusion. These consist almost entirely of coarse (1–2 mm) chromian-spinel grains and at one locality, have been found to contain platinum-group minerals (PGMs).

Olivine clinopyroxenite

Olivine clinopyroxenite is a very coarse-grained rock (up to 20 mm) which forms excellent outcrops in the more elevated areas of the Complex. As with the dunite units, olivine clinopyroxenite is largely devoid of any internal layering or structure. The Southern Intrusion contains three crescent-shaped bodies which vary in width from 10 to over 200 m whereas in the Northern Intrusion, olivine clinopyroxenite comprises a thick (> 350 m) unit which envelops a gabbroic core and occurs as sporadically distributed bands and blocks within the gabbroic sequence.

This rock type consists of 60–95% clinopyroxene and 5–40% olivine. Other than trace amounts of chromian spinel, no other primary minerals are present. All samples examined have adcumulate textures, although the cumulus minerals have subhedral forms due to diffusive creep (Hunter 1996). Zoning is absent from clinopyroxene, except in the easternmost unit of the Southern Intrusion where strong, continuous zoning is ubiquitous. This zoning is suggested to be the result of prolonged cumulus growth without removal of intercumulus liquid.

Volume increase associated with olivine alteration has caused radial fracturing of the surrounding clinopyroxene grains. Clinopyroxene has also undergone mild alteration to amphibole.

Olivine gabbro

Olivine gabbro comprises all of the gabbroic rocks of the Northern Intrusion, but it occurs only as a thin discontinuous band which separates olivine clinopyroxenite from hornblende gabbro-norite in the Southern Intrusion. In all cases, the contact between olivine gabbro and the underlying olivine clinopyroxenite is gradational over distances of between 5 and 50 m. The olivine gabbro sequences are characterised by rhythmically interlayered, plagioclase-rich and plagioclase-poor bands, each of which is only a few centimetres in thickness. Layering is intensely brecciated, folded and slumped at several localities (Fig. 3B, C). These structures are common close to olivine clinopyroxenite units, and we interpret deformation to have resulted from instability of cumulates during solidification due to seismic activity, thermal erosion or magma chamber recharge and venting.

Due to the layering, modal mineral abundances are highly variable. Cumulus phases include clinopyroxene (15–60%), olivine (10–35%) and calcic-plagioclase (5–70%). Cr-rich or Cr-poor titano-magnetite is invariably present in trace amounts. The texture of this rock type is always adcumulate except in the highest levels of the Northern Intrusion where cumulus orthopyroxene and postcumulus hornblende are present, giving the rock a mesocumulate texture. Alteration of olivine and clinopyroxene is identical to that of olivine clinopyroxenite, with radial fractures also apparent in plagioclase grains. Fine grains of anhedral pyrite and chalopyrite are also present but they are rare.

Hornblende gabbro-norite

The core of the Southern Intrusion is composed of hornblende gabbro-norite. Contacts between olivine gabbro and hornblende gabbro-norite are not observed, and we believe that the transition between rock types is manifest as a progressive change in rock mineralogy and texture. In outcrop, hornblende gabbro-norite has many heterogeneous features. Rhythmic layering similar to that observed in the olivine gabbros occurs in many places, and irregular wispy veins of fine-grained mafic melt have invaded the hornblende gabbro-norite host. In some cases, veining comprises up to 40% of the rock and may represent residual melts which were inefficiently extracted from the cumulate pile.

The hornblende gabbro-norites are mostly coarse-grained orthocumulate rocks which display clear poikilitic textures. Primary cumulus minerals include clinopyroxene (10–35%), calcic-plagioclase (30–60%), orthopyroxene (2–10%) magnetite-ilmenite intergrowths ($< 5\%$) and minor olivine. Brown hornblende comprises 10–40% of the rock and is the major postcumulus phase. Anhedral pyrite and chalcopyrite are disseminated throughout the rock but are found only in trace amounts. Alteration manifests as amphibole and chlorite replacement of pyroxene, and pseudomorphing of olivine by magnetite and chlorite.

General geology of the dykes

Gabbro ring dyke

The ring dyke which encloses the Layered Group varies in thickness between 50 and 200 m. Overall it is gabbroic in composition but shows great variation in mineralogy, grain size and texture across the Complex. In all samples, plagioclase and augite are the dominant phases, although olivine, magnetite, orthopyroxene, hornblende, and primary pyrrhotite and chalcopyrite may also be present. Most outcrops consist of equigranular rocks, although porphyritic and cumulate textures are not uncommon. The dyke contains an abundance of xenoliths of hornfelsed country rock and is cut by numerous, smaller mafic dykes. We suggest that the ring dyke was emplaced following cooling and sinking of the Layered Group, and may be analogous to ring dyke complexes exposed in other arc terranes (Clemens-Knott and Saleeby 1999).

Hornblende-anorthite pegmatites

Hornblende-anorthite pegmatite dykes are present throughout the Complex but are most prominent in the ultramafic rocks. They typically manifest as chaotic swarms, forming a network with no preferred orientation, width or grain size. Many dykes exhibit postcumulus textures and banding of plagioclase-rich and hornblende-rich zones. Others contain megacrysts of crescumulate hornblende which may be up to 40 cm in length. These features indicate that melt stagnation and slow cooling occurred during formation of the dykes. Similar dykes have been reported from other arc-related intrusive complexes (Findlay 1969; James 1971; Irvine 1974; Sisson et al. 1996; Clemens-Knott and Saleeby 1999) and are suggested by the current authors to have formed from intercumulus melt which was squeezed out of the ultramafic cumulate pile at a relatively late stage. Due to the heterogeneous and coarse nature of these dykes, a representative bulk sample of their composition could not be taken.

Dolerite and basalt

Dolerite and basalt dykes are present throughout the Complex. All display sharp contacts with their hosts, are typically 0.5 m wide, and are continuous along strike for

up to 400 m. Dyke orientations vary but many have a strike length perpendicular to the gross layering of the Layered Group. Most are equigranular and consist of actinolite and plagioclase in roughly equal proportions, although in some dykes primary clinopyroxene is preserved. Anhedral magnetite, pyrite, chalcopyrite and pyrrhotite are present as minor phases.

Several of the dykes contain plagioclase phenocrysts which vary in grain size from 2 to 10 mm and comprise 10 to 20% of the rock. Although variation in phenocryst composition is evident from oscillatory zoning along the rims, the cores of the crystals are highly calcic (An 91–94). Other phenocrysts are found in the dykes, but their original mineralogy is unknown as they have been completely replaced by secondary amphibole.

Ankaramite

Ankaramite dykes from the Greenhills Complex have been described in detail by Mossman et al. (2000) and are therefore only briefly discussed here. These dykes have intruded the Layered Group, the gabbro ring dyke and the surrounding sediments. All samples studied contain large, euhedral Cr-diopside phenocrysts which have been variably altered to hornblende and tremolite. Phenocrysts of olivine, hornblende and zoned plagioclase are also present in some cases. The groundmass is similar to that of the basaltic dykes, consisting of amphibole and plagioclase.

Other dykes

A small number of trondhjemite and wehrlite dykes cut the ultramafic rocks of the Southern Intrusion. The trondhjemite dykes outcrop in an irregular, anastomosing pattern, are often highly altered and largely consist of oscillatory zoned sodic plagioclase, prehnite, chlorite and quartz. These dykes are likely to have formed from multiple influxes of highly fractionated hydrous melts from the Layered Group. By contrast, the wehrlite dykes are thought to represent primitive magma feeder channels. We interpret the composition and cumulate texture of these dykes to have resulted from interaction of primitive magma with the host dunite.

Mineralogy of the Layered Group

More than 300 analyses of cumulate minerals were made using a JEOL 6400 scanning electron microscope (SEM) equipped with an energy-dispersive spectrometer (EDS), housed at the Research School of Biological Sciences, Australian National University (ANU). Accelerating voltage and counting time were set at 15 kV and 100 s respectively. Additional PGM analyses were conducted with a WDS-equipped Cambax microprobe at the Research School of Earth Sciences, ANU. Fe^{2+} and Fe^{3+} contents for chromian spinel, magnetite, ilmenite and hornblende were calculated assuming stoichiometry.

Olivine

Although rare in hornblende gabbro-norite, olivine is present in all rock types of the Layered Group. All grains are unzoned, but all have been partly altered to serpentine minerals and magnetite or, at higher degrees of alteration, to iddingsite and chlorite. Compositions are forsteritic throughout the cumulate sequences, ranging from $Fo_{92–86}$ in dunite, $Fo_{86–77}$ in olivine clinopyroxenite, $Fo_{78–72}$ in olivine gabbro, to $Fo_{71–67}$ in hornblende gabbro-norite (Table 1). The progressive decrease in forsterite content through the cumulate sequences and the absence of significant compositional gaps between rock types are consistent with the hypothesis that the sequences were formed by fractionation and differentiation of similar parent magmas.

Spinel

Chromian spinel is ubiquitous in the dunites but largely absent from all other rock types of the Complex. The compositional range of 100Cr/(Cr + Al) is 79 to 57

Table 1 Composition of olivine from the Greenhills Complex

Sample	31110[a]	50606	40112	31123[a]	50504	40204
Rock type	Dunite	Dunite	Ol. cpxite	Ol. cpxite	Oliv. gab.	Hble. gab.
Intrusion	Southern	Southern	Northern	Southern	Northern	Southern
SiO_2	41.27	40.84	40.73	39.74	38.47	38.01
FeO	8.84	10.68	13.85	17.01	22.88	28.95
MnO	0.20	0.26	0.26	0.25	0.28	0.52
MgO	49.37	48.37	45.51	42.94	38.21	33.20
CaO	0.03	0.03	0.02	0.01	0.02	0.03
Total	99.71	100.28	100.37	99.95	99.86	100.71
	Molecular formula (based on four oxygens)					
Si	1.01	1.00	1.01	1.01	1.00	1.01
Fe	0.18	0.22	0.29	0.36	0.50	0.64
Mn	0.00	0.01	0.01	0.01	0.01	0.01
Mg	1.80	1.77	1.68	1.62	1.49	1.32
Ca	0.00	0.00	0.00	0.00	0.00	0.00
Fo content	90.87	88.98	85.42	81.82	74.85	67.15

[a]Compositions used for fractionation modelling (Table 8)

(Table 2), and is typical of spinel from island-arc cumulate complexes (Fig. 4) and primitive island-arc volcanic rocks (Barsdell and Berry 1990; Eggins 1993). By contrast, $100Fe^{3+}/(Cr+Al+Fe^{3+})$ signatures, although higher than those of mid-ocean ridge basalts (MORB), range to lower values than many other arc-spinel suites. The Mg# ($100Mg/(Mg+Fe^{2+})$) ranges from 20 to 60, but it is expected to have been affected by subsolidus Fe–Mg exchange during cooling (Ozawa 1984). TiO_2 and MnO were detected in all analyses, but the abundance of these components rarely exceed 0.5 wt%.

Primary magnetite is present within all of the gabbroic cumulates. In the olivine gabbros, it ranges from Cr-rich (9–14 wt% Cr_2O_3) to Cr-poor titano-magnetite which contains up to 5.5 wt% TiO_2 and 4.7 wt% Al_2O_3, and rarely coexists with ilmenite. By contrast, the magnetite found in hornblende gabbro-norite is very pure in composition and is usually associated with small amounts of ilmenite.

Pyroxenes

Pyroxene compositions (Table 3) compare closely with pyroxenes from other island-arc cumulate complexes (Fig. 5). Clinopyroxene ranges from Cr-rich diopside (Mg# 83–91) in olivine clinopyroxenite to Fe-rich diopside and Mg-rich salite (Mg# 76–85) in the gabbroic cumulates. All are low in Na_2O (< 0.3 wt%), TiO_2 (< 0.5 wt%) and Al_2O_3 (1.2–3.6 wt%). Orthopyroxene is relatively rare in the Greenhills Layered Group and only occurs as a minor phase within the hornblende gabbro-norites and some olivine gabbros. Compositions are more primitive in the olivine gabbros (Mg# 75–78) than the hornblende gabbro-norites (Mg# 57–72). Small amounts of CaO (0.6–1.8 wt%), MnO (0.3–0.9 wt%) and Al_2O_3 (0.6–1.6 wt%) are also present. Pigeonite has not been found.

Plagioclase

Although absent from the ultramafic rocks, plagioclase is a major phase in the gabbroic rocks of the Layered Group. Most grains have subhedral forms and are mildly altered along albite or carlsbad twinning planes. Compositions range from $An_{96–88}$ in the olivine gabbros to $An_{91–82}$ in the hornblende gabbro-norites (Table 4) and are typical of island-arc cumulates (Fig. 6). Factors commonly argued to be responsible for crystallisation of such calcic-plagioclase include high magmatic water contents (Arculus and Wills 1980; Sisson and Grove 1993; Panjasawatwong et al. 1997), high melt Ca/(Ca + Na) contents (Panjasawatwong et al. 1997), and low crystallisation pressures (Panjasawatwong et al. 1997). We favour elevated water contents of the parent magma and low crystallisation pressures, as prior crystallisation and fractionation of clinopyroxene would have substantially decreased the Ca/(Ca + Na) ratio of the parental melt.

Amphibole

The presence of magmatic amphibole in some ankaramite dykes (Mossman et al. 2000) and as the principal

Table 2 Composition of Cr-spinel, magnetite and ilmenite from the Greenhills Complex

Sample	33108	33111[b]	33119	32701	33120	50606	50501	40702	50503	51604	40202	51604	51605
Rock type	Dunite	Dunite	Dunite	Dunite	Dunite	Dunite	Oliv. gab.	Oliv. gab.	Oliv. gab.	Hble. gab.	Hble. gab.	Hble. gab.	Hble. gab.
Mineral	Cr-spinel	Cr-spinel	Cr-spinel	Cr-spinel	Cr-spinel	Cr-spinel	Cr Ti-mag	Cr Ti-mag	Ti-mag	Mag	Mag	Ilmenite	Ilmenite
TiO_2	0.35	0.40	0.59	0.22	0.35	1.04	3.47	5.39	3.54	0.93	0.26	50.12	50.39
Al_2O_3	9.67	10.41	12.85	9.30	11.06	20.50	4.16	4.64	1.45	1.60	0.3	0.15	0.08
Cr_2O_3	52.18	51.22	43.16	49.49	48.52	39.55	10.58	13.30	0.46	0.16	–	–	–
Fe_2O_3[a]	7.26	6.82	11.81	7.80	8.43	6.47	45.43	37.84	57.17	61.27	66.62	2.74	1.8
FeO	22.95	23.52	25.27	21.61	22.42	22.54	32.59	34.36	32.56	29.93	29.93	41.89	42.48
MnO	0.69	0.38	0.46	0.63	0.10	0.24	0.41	0.41	0.16	0.08	0.10	0.94	0.92
MgO	6.57	6.41	5.66	6.51	7.09	8.49	0.90	0.48	0.34	0.24	0.35	1.29	1.13
Total	99.67	99.16	99.80	95.56	97.97	98.83	97.54	96.42	95.68	94.21	97.56	97.13	96.80
	Molecular formula (based on four oxygens and Fe^{3+}-corrected)										(based on three oxygens)		
Ti	0.01	0.01	0.02	0.01	0.01	0.03	0.10	0.15	0.11	0.03	0.01	0.97	0.98
Al	0.39	0.42	0.51	0.39	0.45	0.78	0.19	0.21	0.07	0.08	0.01	0.00	0.00
Cr	1.41	1.38	1.16	1.39	1.32	1.01	0.32	0.39	0.01	0.01	0.00	0.00	0.00
Fe^{3+}	0.19	0.18	0.30	0.21	0.22	0.16	1.30	1.10	1.71	1.86	1.97	0.05	0.05
Fe^{2+}	0.65	0.67	0.72	0.64	0.64	0.61	1.03	1.11	1.08	1.01	0.98	0.90	0.92
Mn	0.02	0.01	0.01	0.02	0.00	0.01	0.01	0.01	0.01	0.00	0.00	0.02	0.02
Mg	0.33	0.33	0.29	0.34	0.36	0.41	0.05	0.03	0.02	0.01	0.02	0.05	0.04
Mg#	33.80	32.69	28.53	34.94	36.03	40.17	4.69	2.30	1.83	1.41	2.04	5.26	4.17
Cr#	78.35	76.75	69.26	78.12	74.64	56.41	63.05	65.22	17.55	6.29	–	–	–
Fe^{3+}/Σ^{3+}	9.40	8.87	15.28	10.49	10.99	8.07	72.04	64.64	95.40	95.82	–	–	–

[a]Based on AB_2O_4 stoichiometry for spinel and ABO_3 stoichiometry for ilmenite
[b]Composition used for fractionation modelling (Table 8)

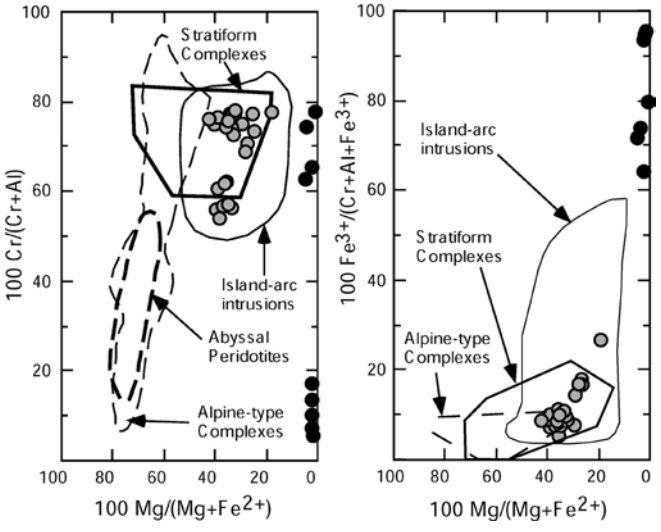

Fig. 4 Composition of chromian spinel (*shaded dots*) and magnetite (*closed dots*) from the Greenhills Complex. Data and fields for other intrusions are from Burns (1985), Jan and Windley (1990), and Himmelburg and Loney (1995)

postcumulus phase in the hornblende gabbro-norites also indicates that the parental melts contained significant water contents. All analysed amphibole grains are magnesio-hornblende in composition (Table 4), with very little octahedral aluminium but significant Fe^{3+} (0.5–1.3 atoms per formula unit). As with pyroxene, hornblende from olivine gabbros (Mg# 90–95) is more primitive than from hornblende gabbro-norites (Mg# 71–86). Detectable levels of Cr_2O_3 (0.04–0.4 wt%) may have been sourced from the breakdown of nearby clinopyroxene, but they are more likely to reflect primitive magma compositions.

Platinum-group minerals

The occurrence of platinum-group minerals (PGMs) from the Greenhills Complex has already been documented (Spandler et al. 2000) and is only briefly described here. PGMs have been identified only from one locality along the southern shoreline of the Complex (Fig. 2) where they are hosted by chromian-spinel schlieren within dunite. Most PGM grains are platinum-iron alloys, very close to pure isoferroplatinum (Pt_3Fe) in composition, although significant levels of Rh and Ir are also present (Table 5). All of these grains are euhedral and are completely enclosed within unzoned chromian spinels. They are interpreted to have crystallised directly from the parent magma in response to a reduction of platinum-group element (PGE) solubility in the magma due to differentiation or variation in oxygen fugacity (Spandler et al. 2000). The only other PGM species identified is sperrylite ($PtAs_2$), of which few grains have been found. These are also very pure in composition, although containing minor Rh and Fe (Table 5). The sperrylite grains occur along chromian-spinel grain boundaries, are anhedral in form, and are suggested to have precipitated during hydrothermal alteration of the host rocks.

The southern shoreline of South Island has long been known for its alluvial PGE mineralisation (Cowden et al. 1990; Mitchell 1995), yet primary sources for the mineralisation remain enigmatic. The alluvial PGM

Table 3 Composition of pyroxenes from the Greenhills Complex

Sample	33121[b]	40112	40116	40119	50501	50503	40110	51605	50504	50506	51604	51605
Rock type	Ol. cpxite	Ol. cpxite	Ol. cpxite	Ol. cpxite	Oliv. gab.	Oliv. gab.	Oliv. gab.	Hble. gab.	Oliv. gab.	Oliv. gab.	Hble. gab.	Hble. gab.
Mineral	Cpx	Cpx	Cpx	Cpx	Cpx	Cpx	Cpx	Cpx	Opx	Opx	Opx	Opx
SiO_2	53.29	53.03	53.28	54.44	52.31	51.08	51.60	52.62	54.01	54.21	53.19	52.41
TiO_2	0.24	0.16	0.17	0.15	0.26	0.68	0.26	0.44	0.41	0.22	0.15	0.23
Al_2O_3	1.77	1.53	1.09	1.06	2.77	3.13	3.34	2.55	1.43	1.47	1.64	1.30
Cr_2O_3	0.28	0.43	0.69	0.70	0.53	0.07	0.43	0.11	0.06	0.12	0.01	0.02
FeO[a]	4.38	3.29	3.77	2.99	5.00	7.41	6.11	8.00	14.42	13.28	17.89	20.43
MnO	0.05	0.02	0.29	0.08	0.00	0.36	0.10	0.33	0.41	0.3	0.61	0.70
MgO	17.32	16.85	17.64	17.73	15.95	14.79	15.34	14.42	27.16	27.84	24.75	22.67
CaO	22.69	23.63	23.13	23.4	22.99	21.92	23.61	22.96	1.13	1.25	1.18	1.83
Na_2O	0.00	0.00	0.01	0.03	0.20	0.32	0.02	0.39	–	–	–	–
Total	100.02	98.94	100.07	100.58	100.01	99.76	100.81	101.82	99.03	98.69	99.42	99.59
	Molecular formula (based on six oxygens)											
Si	1.95	1.96	1.95	1.97	1.92	1.90	1.89	1.93	1.96	1.96	1.96	1.95
Ti	0.01	0.00	0.00	0.00	0.01	0.02	0.01	0.01	0.01	0.01	0.00	0.01
Al	0.08	0.07	0.05	0.05	0.12	0.14	0.14	0.11	0.06	0.06	0.07	0.06
Cr	0.01	0.01	0.02	0.02	0.02	0.00	0.01	0.00	0.00	0.00	0.00	0.00
Fe	0.13	0.10	0.12	0.09	0.15	0.23	0.19	0.24	0.44	0.40	0.55	0.64
Mn	0.00	0.00	0.01	0.00	0.00	0.01	0.00	0.01	0.01	0.01	0.02	0.02
Mg	0.94	0.93	0.96	0.96	0.87	0.82	0.84	0.79	1.47	1.50	1.36	1.26
Ca	0.89	0.93	0.91	0.91	0.90	0.87	0.93	0.90	0.04	0.05	0.05	0.07
Na	0.00	0.00	0.00	0.00	0.01	0.02	0.00	0.03	–	–	–	–
Mg#	87.58	90.13	89.29	91.36	85.04	78.06	81.74	76.26	77.05	78.89	71.15	66.42

[a]Total Fe as FeO
[b]Composition used for fractionation modelling (Table 8)

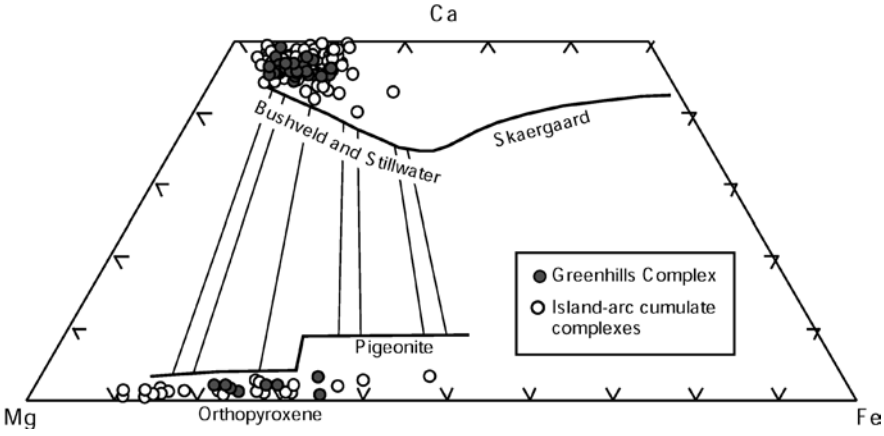

Fig. 5 Pyroxene compositions from the Greenhills Complex and island-arc cumulate complexes. Data for other complexes are from James (1971), Murray (1972), Irvine (1974), Sivell and Rankin (1983), Burns (1985), Jan and Windley (1990), Kepezhinskas et al. (1993), and Himmelburg and Loney (1995). Trends for other layered intrusions are from Irvine (1974)

Table 4 Composition of plagioclase and amphibole from the Greenhills Complex

Sample	40110	50503	50505	50506	51604	51605	40204	50506	40203	40202	51605
Rock type	Oliv. gab.	Oliv. gab.	Oliv. gab.	Oliv. gab.	Hble. gab.	Hble. gab.	Hble. gab.	Oliv. gab.	Hble. gab.	Hble. gab.	Hble. gab.
Mineral	Plagioclase	Plagioclase	Plagioclase	Plagioclase	Plagioclase	Plagioclase	Plagioclase	Horn-blende	Horn-blende	Horn-blende	Horn-blende
SiO_2	44.53	45.00	45.32	45.26	45.22	47.38	46.00	48.55	48.65	49.17	48.65
TiO_2	0.00	0.06	0.00	0.00	0.00	0.00	0.03	0.95	0.65	1.23	1.40
Al_2O_3	35.08	34.97	34.44	34.40	34.63	33.90	34.46	8.64	6.56	6.80	6.24
Cr_2O_3	–	–		–	–	–	–	0.39	0.04	0.09	0.07
Fe_2O_3[a]	–	–		–	–	–	–	6.62	8.36	3.37	11.65
FeO	0.35	0.22	0.48	0.19	0.28	0.00	0.20	1.61	7.76	9.58	4.90
MnO	–	–		–	–	–	–	0.12	0.26	0.19	0.15
MgO	–	–		–	–	–	–	17.74	13.18	15.03	14.01
CaO	19.99	18.71	18.71	17.65	18.19	17.23	18.46	12.18	11.01	11.75	10.44
Na_2O	0.63	0.80	1.00	1.26	1.08	1.80	1.42	1.63	0.86	0.00	1.05
K_2O	0.01	0.00	0.07	0.07	0.03	0.00	0.03	0.13	0.22	0.00	0.13
Total	100.59	99.76	100.02	98.83	99.43	100.31	100.60	98.56	97.55	97.21	98.70
	Molecular formula (based on eight oxygens)							(based on 23 oxygens)			
Si	2.05	2.08	2.10	2.11	2.10	2.17	2.11	6.90	7.20	7.16	7.14
Ti	0.00	0.00	0.00	0.00	0.00	0.00	0.00	0.10	0.07	0.13	0.15
Al	1.91	1.91	1.88	1.89	1.89	1.83	1.87	1.45	1.14	1.17	1.08
Cr	–	–		–	–	–	–	0.04	0.00	0.01	0.01
Fe^{3+}	–	–		–	–	–	–	0.70	0.91	0.37	1.25
Fe^{2+}	0.01	0.01	0.02	0.01	0.01	0.00	0.01	0.19	0.94	1.16	0.59
Mn	–	–		–	–	–	–	0.01	0.03	0.02	0.02
Mg	–	–		–	–	–	–	3.76	2.91	3.26	3.07
Ca	0.99	0.93	0.93	0.88	0.90	0.84	0.91	1.85	1.75	1.83	1.64
Na	0.06	0.07	0.09	0.11	0.10	0.16	0.13	0.45	0.25	0.00	0.30
K	0.00	0.00	0.00	0.00	0.00	0.00	0.00	0.02	0.04	0.00	0.02
An#	94.60	92.82	91.18	88.56	90.27	84.10	87.78				
Mg#								95.17	75.16	73.81	83.59

[a]Based on $A_{0-1}B_2C_5T_8O_{22}(OH)_2$ stoichiometry

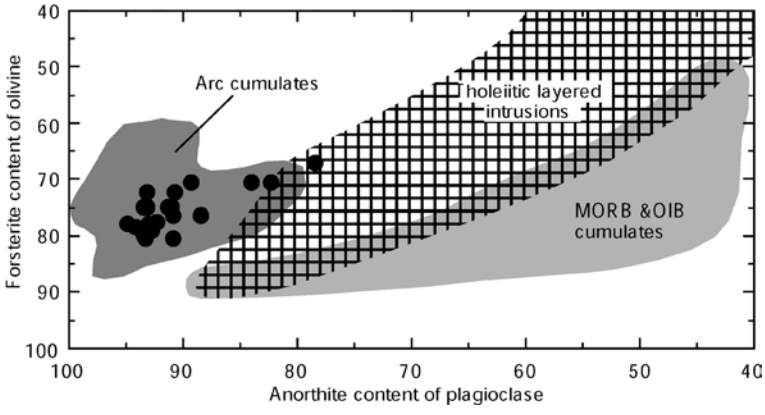

Fig. 6 Composition of coexisting olivine and plagioclase for cumulate rocks of the Greenhills Complex (*closed dots*). *Fields* of arc cumulates, tholeiitic layered intrusions, and MORB and OIB cumulates are from Beard (1986)

Table 5 Composition of platinum-group minerals from the Greenhills Complex and regional placer deposits. Analyses 1–8 are from the Greenhills Complex, analyses 9–11 from regional placer deposits (Mitchell 1995). *B.d.* Below detection limit

No.	1[a]	2[a]	3[b]	4[b]	5[b]	6[a]	7[a]	8[a]	9	10	11
Mineral	Pt–Fe alloy	Pt–Fe alloy	Pt–Fe alloy	Pt–Fe alloy	Pt–Fe alloy	Sperrylite	Sperrylite	Sperrylite	Pt–Fe alloy	Pt–Fe alloy	Sperrylite
Wt%											
Pt	88.26	83.87	89.07	88.15	89.67	56.20	55.06	55.15	89.87	90.20	56.90
Pd	0.61	0.46	0.28	0.42	0.07	0.09	0.18	b.d.	0.56	0.78	–
Rh	1.90	1.82	1.83	1.59	1.50	0.51	1.04	0.24	0.44	1.17	0.28
Ir	1.85	1.35	0.73	1.60	0.57	b.d.	b.d.	b.d.	0.72	1.49	–
Os	0.13	0.21	0.40	–	0.42	b.d.	b.d.	b.d.	b.d.	0.58	–
Fe	8.50	8.27	8.45	8.72	8.94	0.73	0.76	0.72	7.78	4.96	–
Cu	0.39	0.35	–	–	–	b.d.	0.02	b.d.	0.58	0.57	b.d.
S	b.d.	b.d.	–	–	–	0.34	0.46	0.33	–	–	–
As	b.d.	b.d.	–	–	–	42.33	41.39	40.85	–	–	43.70
Total	101.64	96.33	100.76	100.48	101.17	100.20	98.91	97.29	99.95	99.75	100.88
Atomic											
Pt	0.70	0.70	0.72	0.71	0.72	0.33	0.32	0.33	0.74	0.78	0.33
Pd	0.01	0.01	0.01	0.01	0.00	0.00	0.00	–	0.01	0.01	–
Rh	0.03	0.03	0.03	0.02	0.02	0.01	0.01	0.00	0.01	0.02	0.00
Ir	0.02	0.00	0.01	0.01	0.00	–	–	–	0.01	0.01	–
Os	0.00	0.01	0.00	–	0.00	–	–	–	–	0.01	–
Fe	0.24	0.24	0.24	0.25	0.25	0.01	0.02	0.02	0.22	0.15	–
Cu	0.01	0.01	–	–	–	–	0.00	–	0.02	0.01	–
S	–	–	–	–	–	0.01	0.02	0.01	–	–	–
As	–	–	–	–	–	0.64	0.63	0.64	–	–	0.67
Total	1.00	1.00	1.00	1.00	1.00	1.00	1.00	1.00	1.00	1.00	1.00

[a]Analysed by EDS microprobe
[b]Analysed by EDS-equipped scanning electron microscope (SEM)

grains from the eastern beaches occur in very similar modal proportions (Mitchell 1995) and have similar compositions (Table 5) to the PGMs from the Greenhills Complex, indicating that these specific alluvial deposits were sourced from the Greenhills Complex.

Cumulate mineral profiles

Cumulate mineral profiles were constructed to help determine the structure and magmatic evolution of both the Northern and Southern intrusions of the Complex. Data for the profiles were obtained from cumulate samples collected during composite traverses from the margin to the centre of each intrusion and are presented in Fig. 7 (for the Northern Intrusion) and Fig. 8 (for the Southern Intrusion). The total exposed thickness of the Northern Intrusion consists of approximately 350 m of olivine clinopyroxenite overlain by approximately 750 m of olivine gabbro, although the upper 200 m was not examined. The variations in the olivine and clinopyroxene trends through the olivine clinopyroxenite and lower parts of the olivine gabbro sequences are consistent with progressive, in-situ fractional crystallisation and evolution of the parent magma in the magma chamber. The slight trend reversal in the olivine clinopyroxenite may be due to a small influx of more primitive (higher Mg#) magma. Approximately 200 m above the olivine clinopyroxenite–olivine gabbro boundary, there is a pronounced and continuous trend reversal which correlates with the change from Cr-rich to Cr-poor titano-magnetite and the appearance of orthopyroxene. These features cannot be explained by continued fractional crystallisation of the parental magma to the underlying cumulates, and are difficult to reconcile with repeated influx of primitive magma. Instead, we interpret the rocks above the reversal zone to have accumulated from the roof of the magma chamber, i.e. downwards. The differences in mineralogy between the roof and main cumulate sequences indicate that the parental magma underwent compositional stratification after pooling in the chamber. From the composition of magnetite and presence of orthopyroxene, the magma in the roof zone is suggested to have been relatively evolved, and may have been contaminated with residual melts expelled from the main magma reservoir below. However, the dominance of adcumulate textures in the roof cumulate sequence indicates that they also failed to retain residual liquids. The residual liquid may have migrated upwards to be erupted at the surface as volcanic rock. Plagioclase compositions are highly calcic and show little variation throughout the sequence, which we attribute to high water contents in the melt.

Studies of magma chamber dynamics (Marsh 1988, 1995) suggest that the most fractionated rock types in many layered intrusions and sills occur between 65 and 80% of the way up through the cumulate stratigraphy. This would indicate that the total cumulate thickness of the Northern Intrusion exceeded 1.5 km, of which at least several hundred metres remain buried.

The constructed mineral profile for the Southern Intrusion (Fig. 8) includes the entire 2.5-km thickness of the Layered Group, except for the thin olivine clinopyroxenite unit in contact with the gabbroic ring dyke in

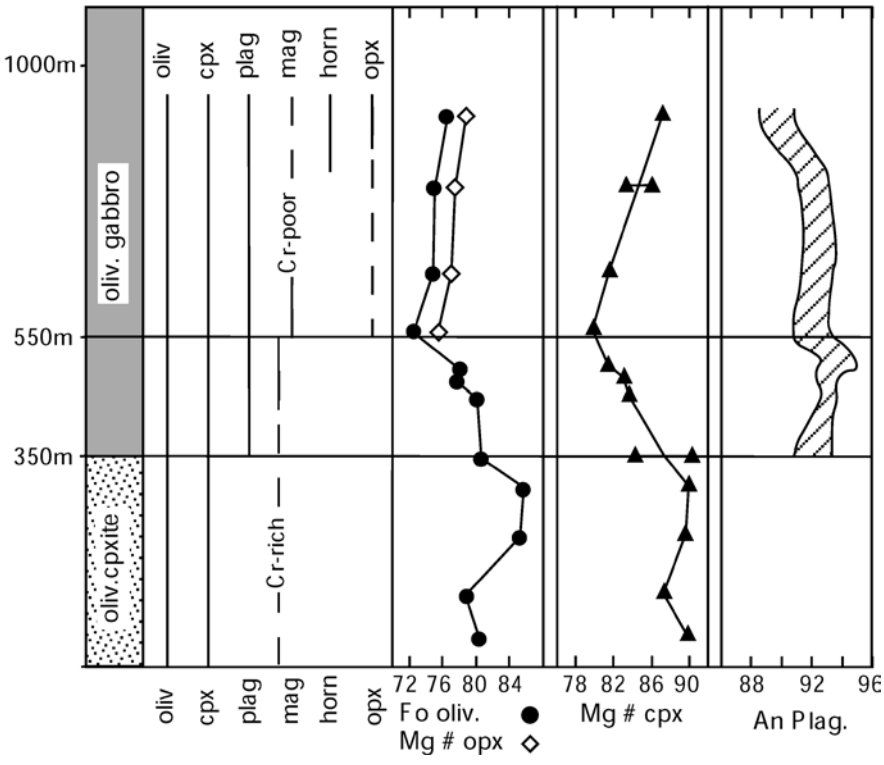

Fig. 7 Exposed cumulate stratigraphy and mineral chemistry trends for the Northern Intrusion of the Greenhills Complex. Patterns in the key column correlate to the rock-type key of Fig. 2. Mineral abbreviations: *oliv* olivine, *cpx* clinopyroxene, *plag* plagioclase, *mag* magnetite, *horn* hornblende, *opx* orthopyroxene, *Cr-sp* Cr-spinel

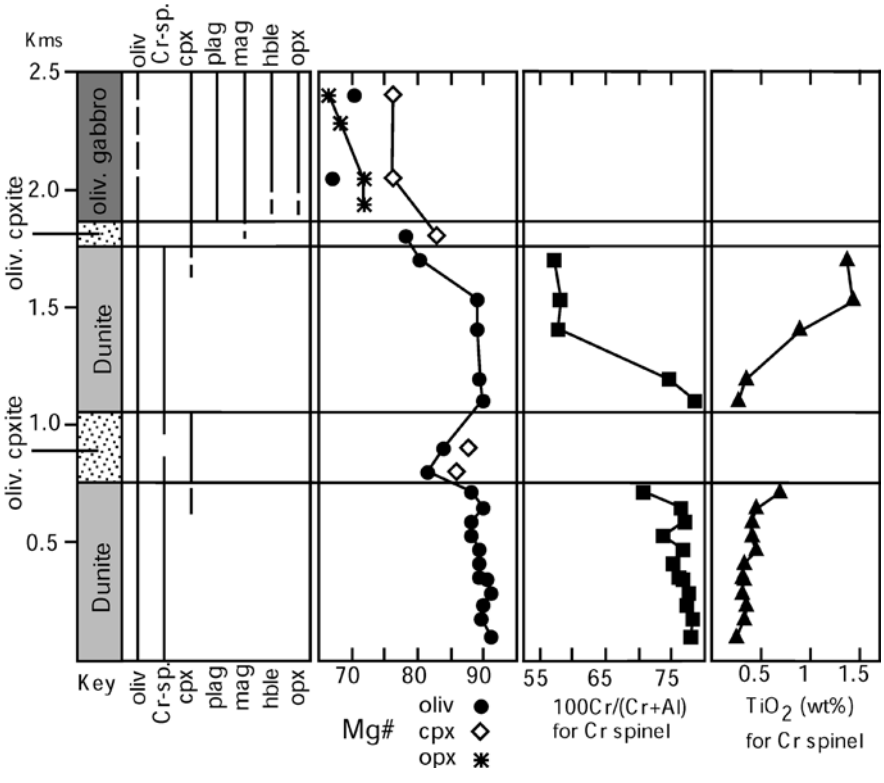

Fig. 8 Exposed cumulate stratigraphy and mineral chemistry trends for the Southern Intrusion of the Greenhills Complex. Patterns in the key column correlate to the rock-type key of Fig. 2. Mineral abbreviations are as in Fig. 7

the east of the Complex. It is unclear whether this unit formed as part of the Layered Group or during intrusion of the ring dyke. The easternmost (lower) dunite sequence consists of highly primitive cumulus minerals (high Cr# and low TiO_2 of spinel, and high Fo contents) and represents the earliest-formed cumulates of the Complex. The large thickness and absence of fractionation trends through this unit is interpreted to be due to small but periodic influxes of primitive magma into the chamber. These small melt influxes must have ceased by

the time the central olivine clinopyroxenite unit was accumulating, as this unit consists of more evolved mineral compositions. However, an abrupt change to highly primitive mineral compositions at the base of the overlying dunite unit indicates that the magma chamber was replenished by a large volume of hot, primitive magma. Turbulent mixing of the primitive and residual melts, and thermal erosion of cumulates at the base of the chamber are evident from the complex, intermixed contact between the central olivine clinopyroxenite and upper dunite units. Progressive magmatic differentiation with minimal further melt recharge during formation of the upper cumulate sequences is reflected through trends of increasing TiO_2 and decreasing Cr# of chromian spinel, decreasing Fo content of olivine (for the upper dunite and upper olivine clinopyroxenite units), and decreasing Mg# of orthopyroxene (in the gabbroic rocks). The orthocumulate texture of the hornblende gabbro-norites and zoning of minerals in the upper olivine clinopyroxenite unit indicate that residual melts were not effectively removed during crystallisation and compaction of these cumulates.

Summary

The crystallisation sequence and mineral compositions of the Layered Group are typical of mafic to ultramafic cumulate blocks reported from island arcs. The Mg and Ca-rich composition of the minerals indicates that the parent magmas were derived from a primitive source. Highly calcic plagioclase and the abundance of hornblende in some gabbroic rocks and dykes (Mossman et al. 2000) are consistent with high water contents in the magmas (Sisson and Grove 1993). High chromium and low aluminium contents of chromian spinel, clinopyroxene, hornblende and some magnetite suggest that the parent magma remained relatively primitive, despite significant in-situ fractionation. Field relations and cumulate mineral profiles for each intrusion reveal a complex history of magmatic differentiation, magma mingling and cumulate formation within the magma chambers. The Northern Intrusion is suggested to consist of two separate cumulate sequences (main and roof) which formed after ponding and magma stratification in the chamber. Both of these sequences effectively expelled residual melts, some of which may have erupted to form volcanic rock. The Southern Intrusion formed as a single cumulate sequence, but it was subject to many influxes of primitive magma at the early stages of cumulate production. The mineralogy and texture of the most fractionated rock types of this intrusion indicate that residual melts were inefficiently removed.

Cumulate and melt geochemistry

Many of the dykes of the Greenhills Complex are suggested to represent magmas which were responsible for formation of the Layered Group (Spandler et al. 2000). Therefore, the composition of 24 cumulates and nine mafic dykes were determined in order to evaluate the chemical evolution of the parent magmas and cumulates of the Complex. Major and trace elements for the cumulates, and major elements, Cr, Ni, and Pb for the dyke samples were determined in duplicate using a Philips PW2400 wavelength-dispersive X-ray fluorescence (XRF) spectrometer and a Spectro X-Lab energy-dispersive XRF (for Pb), both housed at the Department of Geology, ANU. Major elements were measured using 30-mm-diameter, Li borate glass fusion discs. Trace-element analysis was conducted on a pressed disc containing 5 g of rock powder and a small amount of 2% PVA solution. All other trace-element concentrations were determined by laser ablation, inductively-coupled plasma mass spectrometry (LA ICP-MS) at the Research School of Earth Sciences, ANU. The LA ICP-MS employs an ArF (193 nm) Excimer laser and a Fisons PQ2 STE ICPMS. A spot size of 100 μm was used, and counting time was set at 70 s. Instrument calibration was against NIST 612 glass, and background analysis time was 60 s. ^{43}Ca was employed as the internal standard isotope, based on CaO concentrations previously measured by XRF. Loss-on-ignition (LOI) values were calculated from the mass difference to 2 g of powdered sample after heating to 1,010 °C for one hour.

The spinel-hosted, multiphase inclusions are believed to represent samples of primary or near-primary magma which was parental to the Layered Group (Spandler et al. 2000). Therefore, knowledge of their composition is also important for determining the magmatic evolution of the Complex. Prior to analysis, melt inclusion samples were homogenised following the procedures outlined by Spandler et al. (2000). The inclusions were then analysed for major elements by EDS-equipped SEM, and for trace elements by LA ICP-MS. A spot size of 35 μm and counting time of between 30 and 90 s were used for the LA ICP-MS analyses.

Representative analyses of the cumulates and dykes and melt inclusions are presented in Tables 6 and 7 respectively. Samples of similar lithology from both intrusions do not have significant compositional differences, implying both intrusions crystallised from common parent magma. The melt inclusions have ankaramitic affinities ($1 < CaO/Al_2O_3$; Della-Pasque and Varne 1997) and are very similar in composition to the ankaramite dykes, with the notable exception of Na_2O, MgO, FeO and MnO contents. We cannot account for the differences in Na_2O but suspect problems associated with analysing such small melt inclusions. The melt inclusions are likely to have suffered subsolidus Fe–Mg–Mn exchange with their host spinel during cooling, and therefore have lower MgO and higher FeO and MnO contents than expected. Most of the other dykes have major-element characteristics of high-alumina basalts (HAB) as defined by Crawford et al. (1987). The cumulates have compositions which reflect their primary mineralogy, except in the case of dunite which has high

Table 6 Major-element oxide (in wt%) and trace elements (in ppm) for cumulate rock from the Greenhills Complex. The number of decimal places indicate the appropriate level of precision

Sample	33006	51606	51602	51607	40107	40119	40115	40110	50506	33002	40603	51604	51605
Rock type	Dunite	Dunite	Ol. cpxite	Ol. cpxite	Ol. cpxite	Ol. cpxite	Ol. gab.	Ol. gab.	Ol. gab.	Hble. gab.	Hble. gab.	Hble. gab.	Hble. gab.
Intrusion	Southern	Southern	Northern	Southern	Northern	Northern	Northern	Northern	Northern	Southern	Southern	Southern	Southern
SiO_2	38.70	37.37	49.99	47.41	50.95	50.29	44.99	43.97	45.69	46.88	47.44	46.73	46.06
TiO_2	0.09	0.04	0.16	0.13	0.24	0.13	0.20	0.11	0.27	0.91	0.87	0.42	1.13
Al_2O_3	1.50	0.41	2.01	1.72	3.26	1.51	11.15	22.23	8.80	10.12	20.96	22.96	17.88
Fe_2O_3[a]	12.28	11.67	6.81	9.28	7.70	7.13	8.80	5.65	11.50	16.69	11.26	9.66	13.78
MnO	0.19	0.18	0.14	0.17	0.17	0.15	0.16	0.09	0.21	0.27	0.24	0.20	0.21
MgO	41.53	44.03	21.08	25.51	18.40	20.91	17.80	10.50	18.86	13.11	6.29	7.62	7.37
CaO	1.21	0.38	18.19	14.33	18.35	18.55	14.34	15.60	13.62	11.56	11.09	12.19	12.16
Na_2O	0.08	0.00	0.12	0.10	0.42	0.11	0.47	0.51	0.41	0.79	1.38	0.75	1.43
K_2O	0.00	0.00	0.00	0.00	0.03	0.00	0.01	0.02	0.03	0.06	0.09	0.03	0.09
P_2O_5	0.00	0.00	0.00	0.00	0.01	0.00	0.00	0.00	0.01	0.02	0.03	0.00	0.02
S	0.01	0.01	0.01	0.01	0.01	0.01	0.01	0.01	0.01	0.01	0.01	0.00	0.01
LOI	4.87	6.52	2.00	2.32	–	1.71	2.81	1.66	1.66	0.10	0.88	0.32	0.47
Total	100.46	100.61	100.51	100.99	99.54	100.50	100.74	100.35	101.07	100.52	100.54	100.88	100.61
Cr	2,300	2,580	2,240	1,850	1,920	2,220	985	396	830	339	11	38	88
Ni	1,170	1,100	288	410	158	252	257	110	188	91	28	50	36
Sc	12	8	74	84	77	74	53	30	76	87	34	24	64
V	38	22	120	108	160	119	111	61	132	396	280	182	440
Sr	14.0	0.7	13.5	9.1	27.0	9.5	87	160	79	89	281	254	193
Y	1.0	0.7	5.3	3.9	7.0	3.0	4.0	2.0	7.2	9.0	4	2.3	10.0
Zr	2.0	0.5	3.3	3.7	7.0	1.0	4.0	2.0	9.1	15.0	18	3.3	16.3
Ba	1.0	1.1	1.2	1.6	0.1	0.0	0.2	0.0	5.7	10.0	28	13.3	27.5

[a]Total Fe as Fe_2O_3

LOI values due to serpentinisation. However, serpenitinsation is not expected to have significantly altered the relative proportions of most major and minor elements (Coleman and Keith 1971). The LOI values calculated for most of the other samples are less than 2 wt%, indicating that metamorphic and hydrothermal alteration was limited. Therefore, we use LOI-excluded data normalised to 100% for construction of element variation diagrams in Fig. 9. These diagrams plot elements against MgO in log scale to illustrate geochemical trends with magmatic differentiation and progressive cumulate formation.

Given the constraints outlined above, the cumulates, melt inclusions and dykes define general trends which are consistent with progressive removal of cumulate phases from magmas which are represented by the melt inclusions and dykes. For example, highly compatible element trends (Cr and Ni) decrease in smooth, linear fashion with differentiation on the log–log plots, as expected for layered intrusions formed by fractionation of evolving mafic magma. The influence of clinopyroxene and plagioclase crystallisation on magma evolution can be seen in the CaO and Al_2O_3 trends. Early depletion of Ca from the melt is due to extensive clinopyroxene crystallisation, which accumulated to form olivine clinopyroxenite. Arrested Ca depletion from the melt at lower MgO contents (< 7 wt%) is inferred to be due to plagioclase saturation and a decreased proportion of clinopyroxene crystallisation. The relatively late crystallisation of plagioclase also accounts for the low Al contents of the ultramafic rocks and pronounced enrichment of Al in the melts. This enrichment appears to have continued even after plagioclase saturation, as the most evolved dykes have Al contents which exceed values observed in the cumulates. Incompatible oxides, represented by the TiO_2 and K_2O plots, have trends of enrichment with differentiation, as may be expected for cumulate complexes. The lack of TiO_2 depletion also suggests that the large-scale magnetite crystallisation and accumulation did not occur at Greenhills. Retention of residual liquids in the hornblende gabbro-norites is further supported by the fact that their compositions are similar to those of the melt samples. However, all melt samples have significantly higher K_2O contents than the hornblende gabbro-norites, indicating that the latter have lost some of their residual melt.

Trace-element characteristics of the melt inclusions and dykes are presented in Fig. 10. The melt inclusions and ankaramite dykes have very similar trace-element signatures, and are suggested to represent the composition of primitive parent magmas of the Complex. They have elevated large-ion lithophile element contents relative to high field strength elements, have slightly light REE-depleted REE patterns, and are classified as low-K island-arc tholeiite magmas (Spandler et al. 2000). This is consistent with the assemblage and chemistry of the cumulate minerals, as outlined above, and the inferred regional geological setting (Frost and Coombs 1989; Houghton and Landis 1989).

More evolved mafic dykes (Fig. 10B) have higher trace-element contents but retain a similar geochemical signature to the melt inclusions and ankaramite dykes. This supports a direct genetic relationship between all of the melt samples, and indicates that most trace elements

Table 7 Major-element oxide (in wt%) and trace-element (in ppm) data for melt inclusions and dykes from the Greenhills Complex and basalts from the Takitimu Mountains and Riverton Peninsula. The number of decimal places indicate the appropriate level of precision

Location	South. Int.	South. Int.	South. Int.	South. Int.	North. Int.	North. Int.	North. Int.	North. Int.	South. Int.	South. Int.	South. Int.	Taki-timu	Taki-timu	Riverton
Sample type	Melt inclusions				Ankaramites		Dolerite	Basalt	Dolerite	Dolerite	Basalt	Basalt	Basalt	Basalt
Sample no.	M1	M2	M4	M5	32802	40102	40701	40117	40404	40302	33009	51301	51302	32910A
SiO_2	46.54	46.94	47.40	47.93	48.94	49.17	48.99	49.47	51.36	49.04	49.58	45.95	51.50	49.75
TiO_2	0.80	0.51	0.72	0.47	0.41	0.45	0.84	0.65	1.13	0.95	0.92	0.81	0.92	0.99
Al_2O_3	10.27	8.38	9.24	9.11	9.55	10.05	19.23	14.04	17.16	16.56	17.96	17.42	16.98	15.57
Fe_2O_3[a]					10.16	10.29	11.12	9.98	11.80	10.75	10.66	10.27	9.10	10.74
FeO[b]	12.85	12.85	9.72	12.75										
MnO	0.40	0.52	0.34	0.46	0.19	0.19	0.19	0.18	0.19	0.19	0.17	0.17	0.15	0.15
MgO	12.18	12.02	12.57	12.75	16.18	15.87	4.59	9.77	5.05	5.96	6.72	8.36	4.23	7.47
CaO	14.19	16.04	15.92	14.89	12.37	11.52	10.62	10.98	9.73	9.71	10.04	11.12	8.40	7.45
Na_2O	3.01	2.32	3.11	2.52	1.09	1.20	2.81	2.28	2.52	3.17	2.84	2.39	2.52	4.16
K_2O	0.22	0.18	0.31	0.17	0.22	0.32	0.78	0.46	0.35	0.92	0.40	0.37	1.48	0.8
P_2O_5	–	–	–	–	0.03	0.03	0.061	0.06	0.08	0.12	0.08	0.11	0.20	0.132
S	–	–	–	–	0.02	0.01	0.06	0.00	0.03	0.01	0.02	0.01	0.16	0.01
LOI	–	–	–	–	1.09	1.10	0.55	2.42	0.73	2.87	0.62	3.86	4.90	–
Total	100.46	99.76	99.33	101.05	100.25	100.20	99.85	100.30	100.12	100.25	100.01	100.82	100.53	97.22
Cr	–	–	–	–	950	880	9	120	16	124	35	98	42	52
Ni	–	–	–	–	254	270	8	82	8	50	33	74	22	46
Sc	–	–	–	–	54.41	50.04	49.15	56.57	43.66	38.81	35.36	33.65	23.31	39.05
Ti	3,602	2,159	2,887	2,022	2,396	2,702	4,901	3,856	6,615	5,555	5,386	4,176	4,597	5,811
V	–	–	–	–	228	217	324	268	370	319	283	247	222	316
Rb	3.25	2.68	5.58	4.16	4.00	6.00	45.27	68.45	41.23	87.16	53.06	4.04	19.55	91.92
Sr	94.6	77.4	101	89.8	91.7	113	209	350	206	422	271	348	823	468
Y	12.20	8.66	19.07	7.98	10.38	11.83	21.23	16.06	19.27	20.95	16.69	15.86	19.63	21.90
Zr	15.89	11.11	17.53	10.20	14.92	17.99	30.97	35.40	34.54	57.73	35.24	37.65	75.89	63.55
Nb	0.33	0.25	0.31	0.24	0.49	0.53	0.66	0.80	1.32	1.37	0.96	1.41	1.89	1.54
Cs	0.21	0.27	0.86	0.60	0.60	1.13	1.82	0.80	0.54	1.11	0.76	0.22	0.25	0.31
Ba	36.3	29.9	55.1	44.0	43.0	61.2	94.3	120	57.5	197	54.1	43.8	141	115
La	0.83	0.87	0.78	0.69	1.06	1.20	2.03	2.95	3.17	4.87	3.01	3.87	7.03	4.06
Ce	2.29	2.92	2.63	1.91	2.37	2.83	4.74	6.65	7.87	11.25	6.65	8.65	16.09	10.25
Nd	2.50	2.81	3.38	1.90	2.46	2.72	4.72	5.07	6.28	8.73	5.61	6.89	12.05	8.58
Sm	1.15	0.63	1.46	0.68	0.83	1.00	1.77	1.80	2.00	2.48	1.84	2.15	3.20	2.66
Eu	0.39	0.23	0.60	0.27	0.32	0.43	0.71	0.59	0.82	0.92	0.69	0.75	1.03	0.97
Gd	1.68	1.00	2.13	0.95	1.43	1.52	2.68	2.28	2.73	3.26	2.41	2.42	3.36	3.21
Dy	2.44	1.59	3.55	1.44	1.79	1.94	3.58	2.64	3.33	3.58	2.84	2.65	3.26	3.88
Er	1.43	0.93	2.47	0.88	1.16	1.35	2.29	1.74	2.02	2.34	1.86	1.65	1.92	2.39
Yb	0.99	0.68	2.10	0.61	1.14	1.31	2.37	1.66	1.95	2.19	1.69	1.58	1.96	2.37
Lu	–	–	–	–	0.19	0.21	0.39	0.24	0.31	0.36	0.28	0.25	0.32	0.34
Hf	–	0.55	0.84	–	0.54	0.65	1.11	1.10	1.36	1.74	1.14	1.18	2.04	1.96
Ta	–	–	–	–	0.05	0.06	0.06	0.08	0.13	0.12	0.08	0.10	0.11	0.12
Pb	1.87	3.74	3.00	3.63	2.30	10.25	3.0	3.7	4.5	4.7	2.7	4.2	6.0	1.8
Th	0.09	0.08	0.06	0.08	0.14	0.18	0.25	0.63	0.42	1.23	0.52	0.50	0.65	0.22
U	0.02	0.04	0.04	0.02	0.09	0.11	0.14	0.17	0.22	0.44	0.23	0.26	0.52	0.13

[a]Total Fe as Fe_2O_3
[b]Total Fe as FeO

are not strongly fractionated relative to each other during magmatic differentiation. An exception is the progressive enrichment of light REEs relative to heavy REEs. This is most likely due to fractionation of olivine and clinopyroxene, both of which preferentially incorporate heavy REEs over light REEs (Rollinson 1993; Green 1994), and may in part account for the light-REE enrichment observed in some arc lavas.

As outlined above, the Greenhills magma chambers were likely to have been periodically recharged with primitive magma, causing expulsion and eruption of residual melts to form volcanic rocks. The evolved mafic dykes may be representative of such volcanic rocks, but there are no known volcanic sequences which can be directly correlated with the Greenhills Complex. Fortunately, well-preserved volcanic and volcaniclastic sequences of Brook Street Terrane affinities are located within the region (Fig. 1). Interbedded pillow basalts and tuffs are well exposed along the Riverton Peninsula, 25 km north-west of the Greenhills Complex (Challis and Lauder 1977), and a thick succession of mafic to intermediate lavas and volcaniclastic sediments comprises the Takitimu Mountains, a further 60 km to the north (Houghton 1981). For comparative purposes, we have determined the composition of representative samples of aphyric pillow basalts from the Riverton Peninsula and basalt flows from the southern Takitimu Mountains, following the same analytical procedures

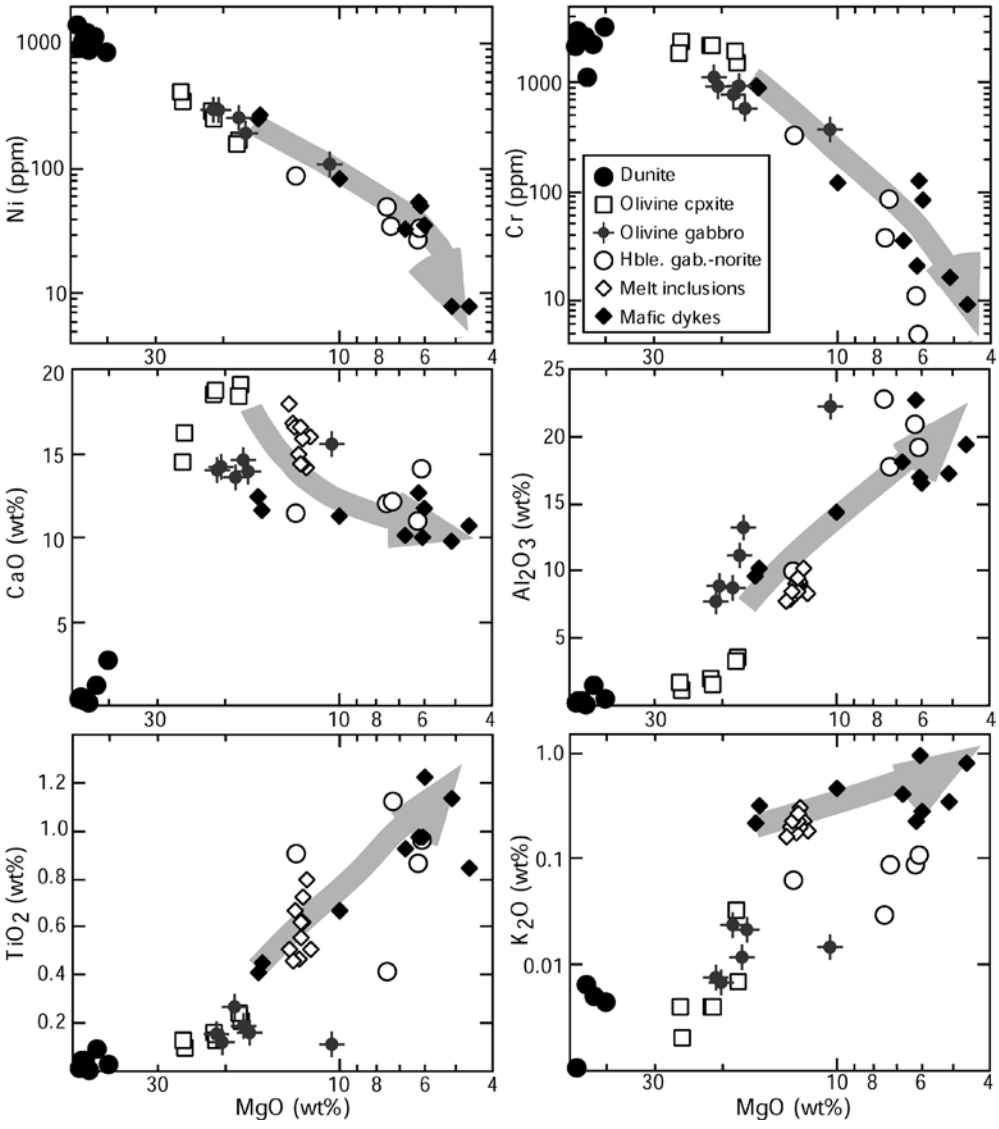

Fig. 9 Selected major- and trace-element variation diagrams for cumulate rocks, dykes and melt inclusions from the Greenhills Complex. The *shaded arrows* represent inferred trends of magmatic differentiation

used for dykes from the Greenhills Complex. Data for three of these samples are presented in Table 7. The lavas are comparable to the mafic dykes from Greenhills for most major elements, although there are some notable exceptions. Of the Takitimu samples, one is low in silica and both are inferred to be volatile-rich from high LOI values. All of the Riverton pillow basalts have high Na_2O contents, which is attributed to seawater alteration during and after eruption (Staudigel et al. 1996). Trace-element characteristics (Fig. 11) are remarkably similar for samples from all three areas, consistent with a genetic relationship. The differences in Cs, Rb, and Ba and relatively high LOI values (for the Takitimu samples) are attributed to mobilisation of these elements during low-grade metamorphism or hydrothermal alteration. Nonetheless, it is clear that the mafic dykes cutting the Greenhills Complex are likely to be analogous to volcanic rocks which erupted above the Complex. Furthermore, we suggest that the volcanic rocks of the Riverton Peninsula and Takitimu Mountains were formed after significant magmatic differentiation in magma chambers similar to those of the Greenhills Complex.

Discussion

The field evidence, petrography and whole-rock geochemistry presented above indicate that early and progressive fractionation of olivine (+ Cr-spinel) and clinopyroxene from an ankaramitic parent melt may generate derivative HAB. As cumulus minerals of the ultramafic rocks have limited compositional variation, simple forward modelling was conducted based on the composition and proportions of cumulus minerals in the cumulates (Table 8). Using an ankaramite dyke as a starting composition (Table 7) and representative cumulus minerals (Tables 1, 2, and 3), we have calculated the composition of the residual liquid after 10% fractionation of olivine and spinel (proportions 99:1),

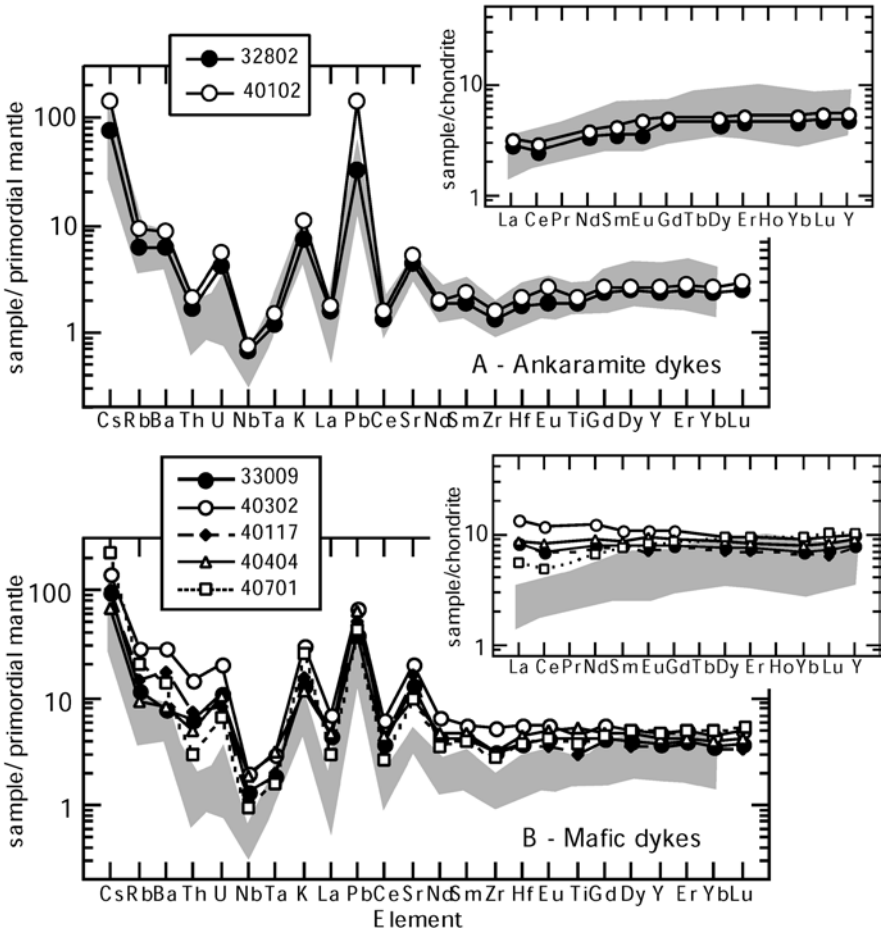

Fig. 10A, B Normalised trace-element diagrams for **A** melt inclusions (*shaded field*; after Spandler et al. 2000) and ankaramite dykes, and **B** melt inclusions (*shaded field*) and other mafic dykes from the Greenhills Complex. Primordial-mantle and chondrite normalisation data are taken from Sun and McDonough (1989), and Taylor and McClennan (1981) respectively

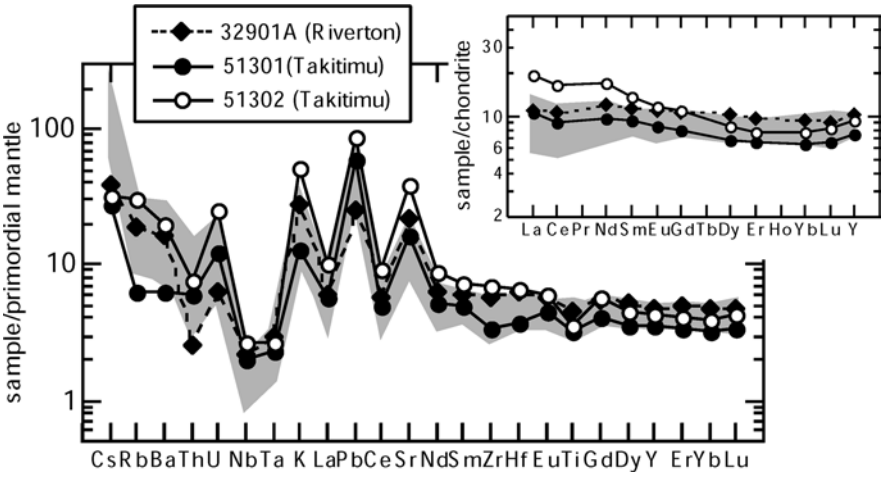

Fig. 11 Normalised trace-element diagram for basalts from the Takitimu Mountains and Riverton Peninsula and evolved mafic dykes from the Greenhills Complex (*shaded field*). Data for normalisation are as in Fig. 10

followed by a further 42% fractionation of olivine and clinopyroxene (proportions 20:80). The resulting liquid is remarkably similar to the average composition of the HAB dykes from the Greenhills Complex (Table 8). As a further test, we have also employed the petrologic program MELTS (Ghiorso and Sack 1995) to model low pressure (0.3 GPa) fractionation of ankaramite. Using MELTS, clinopyroxene saturation is reached after ~12% crystallisation of olivine and spinel (99:1) from the melt. This is comparable with our own estimates for the point of clinopyroxene saturation. Furthermore, calculated liquid compositions at clinopyroxene saturation are also very similar using the two methods. Problems were experienced with further fractionation modelling using MELTS, as unreasonable olivine-clinopyroxene proportions are calculated. Nonetheless, after a further 45% crystallisation (of mostly clinopyroxene), a comparable HAB residual liquid is produced (Table 8).

Table 8 Crystal fractionation modelling

	Starting comp.	Calc. melt at cpx saturation		Calc. HAB melt		Average HAB dyke
	32802[a]	Cumulus mins.	MELTS	Cumulus mins.	MELTS	Greenhills Complex
Temp. (°C)			1,250		1,150	
F	0	0.1	0.125	0.52	0.57	
Min. crystallised		Oliv, Cr-sp	Oliv, Cr-sp	Cpx, oliv	Cpx, oliv	
Proportions		99:1	99:1	80:20	97:3	
(wt%)						
SiO_2	49.72	50.69	50.53	50.77	51.33	50.24
TiO_2	0.42	0.46	0.47	0.66	0.65	0.95
Al_2O_3	9.70	10.77	10.97	17.54	17.33	18.12
Cr_2O_3	0.13	0.09	0.1	0.00	0.03	0.00
Fe_2O_3	2.06	2.29	2.30	3.94	2.02	2.24
FeO	7.43	7.25	6.92	7.51	6.74	8.06
MnO	0.19	0.19	0.18	0.27	0.31	0.19
MgO	16.44	12.81	11.72	5.83	6.49	6.29
CaO	12.57	13.96	14.16	10.93	9.84	10.51
Na_2O	1.11	1.23	1.25	2.12	2.40	2.82
K_2O	0.22	0.25	0.25	0.43	0.52	0.58
H_2O	–	–	1.15	–	2.35	–
(ppm)						
Ni	254	72–176		15–150		8–50
Sr	91	101		146		206–422
Ba	43	48		82		54–197
Y	10.38	12		15		16–21
Zr	14.92	16		28		31–58

[a]Ankaramite dyke sample 32802 (Table 7) is used as the starting composition. The cumulus minerals model uses representative cumulus mineral composition (Tables 1, 2, 3) and mineral proportions from the ultramafic cumulates. For MELTS modelling (Ghiorso and Sack 1995), pressure was set to 0.3 GPa, starting oxygen fugacity to FMQ +2, and starting melt water content to 1 wt%. Fe^{3+}:Fe^{2+} ratios were set to 1:4. All compositions are normalised to 100% major-element oxides. Trace-element calculations utilise olivine-melt and clinopyroxene-melt partition coefficients from Rollinson (1993). Mineral abbreviations are as in Fig. 7. F, total fraction of the starting melt crystallised

The excellent correlation between modelled melt evolution using MELTS and cumulate mineral composition and the Greenhills HAB dykes supports our suggestion that ankaramitic magmas may evolve to HAB through progressive fractionation (~50% crystallisation) of olivine and clinopyroxene, with dunite and olivine clinopyroxenite cumulates forming from concentration of the fractionating phases. One discrepancy is the difference between the apparent relative proportions of dunite and olivine clinopyroxenite in the complex (~1:1) compared with the proportion of the rock types which is expected from the modelling (~1:4). We propose two reasons to account for this discrepancy. Firstly, true proportions of rock types in the Complex are difficult to estimate, as only two dimensions are generally observable. Secondly, fractionation modelling does not account for magma recharge, magma mixing and magma stratification, all processes which have influenced the formation of the Complex. Most notably, the broad and disproportionate thickness of the lower dunite unit of the Southern Intrusion has already been suggested to result from repeated influxes of primitive magma.

The occurrence of ankaramitic melt inclusions and dykes in the Greenhills Complex adds to the growing body of evidence suggesting that highly calcic, subduction-zone magmas may represent true melt compositions (Barsdell and Berry 1990; Della Pasqua and Varne 1997; Sisson and Bronto 1998; Schiano et al. 2000). Nonetheless, the origin of this magma type remains controversial. Some authors have favoured fusion of lower-crustal wehrlites or clinopyroxenites (Barsdell and Berry 1990; Sisson and Bronto 1998; Schiano et al. 2000) and others invoke melting of mantle peridotite which was previously metasomatised by slab-derived carbonatite melt (Green and Lus 2000) or CO_2-rich fluids (Della Pasqua and Varne 1997). There is no record of calcareous nanoplankton or Foraminifera prior to the Triassic (Lipps 1970), indicating that carbonates were not a major component of the sedimentary material drawn into subduction zones. Furthermore, mobilisation of inorganic carbonate from deeper levels of the subducting slab is unlikely to significantly contribute to arc magmatism. As a consequence, the source of the Greenhills parent magmas would not have been altered by carbonatite melt or CO_2-rich fluids. Therefore, we suggest that the Greenhills parent magmas were formed from high-percentage melting of a very primitive, clinopyroxene-rich source which was not affected by CO_2-bearing fluids or melts. Under these conditions, the relatively low trace-element contents of the Greenhills parent magmas are unexpected, as clinopyroxene is the principal host for many trace elements (including REEs) in mantle peridotites (Eggins et al. 1998). However, clinopyroxenite or wehrlite which have previously formed as cumulate assemblages at the base of an island arc may be relatively depleted in trace elements and

hence a viable source for such magmas. High-percentage melting of such rocks is also expected to produce magmas which contain elevated PGE contents, accounting for the magmatic PGMs which occur in the Complex. We note that the discovery of PGMs in cumulates related to tholeiitic arc magmas represents a new provenance for these types of mineral assemblages. However, it is clear that only the most mafic parts of comparable cumulate sequences are likely to contain PGMs.

The origin of HAB is also highly controversial. These are a common rock type found in island arcs, yet it is unclear whether they represent primary magmas formed from melting of the subducted slab (Brophy and Marsh 1986; Myers and Johnston 1996) or are products of fractionation of a primitive basaltic parent melt (Murray 1972; Perfit et. al. 1980; Crawford et. al. 1987; Sisson and Grove 1993). The rocks of Greenhills Complex provide convincing evidence that high-Mg parent magmas (in this case, of ankaramite affinities) can evolve to HAB through progressive crystallisation of olivine (+ Cr-spinel), and olivine and clinopyroxene. This fractionation trend is compatible with those suggested from experimental work on HAB genesis (Crawford et al. 1987; Sisson and Grove 1993), although the HAB dykes from Greenhills lack the high water contents and phenocryst abundance predicted from experiments. It is clear that the parent magmas were hydrous, so we suggest that volatile components were lost during dyke emplacement, preventing phenocryst growth.

Many of the world's exposed ultramafic/mafic island-arc cumulate complexes are concentrically zoned, Alaskan-type intrusions. These intrusions have mineral assemblages and compositions similar to those described for the Greenhills Complex, except that they typically contain more hornblende and magnetite (Murray 1972; Himmelburg and Loney 1995). These differences indicate that the Greenhills parent magmas were less hydrous, less oxidised and less alkaline than the parent magmas of typical Alaskan-type complexes. The unusual concentric structure of Alaskan-type intrusions has been attributed to rapid vertical magma flow in extensional tectonic environments or along major crustal-scale fault zones (Snoke et al. 1982; Johan et al. 1989; Kepezhinskas et al. 1993; Tistl et al. 1994). These tectonic conditions may have favoured post-emplacement unroofing of the arc and may account for the relative abundance of Alaskan-type complexes exposed at the present time.

Other well-documented arc cumulate complexes occur within the Kohistan Terrane of North Pakistan (Jan and Windley 1990; Khan et al. 1993) and in the Border Ranges Mafic/Ultramafic Complex of southern Alaska (Burns 1985; DeBari and Coleman 1989). Again, these complexes share many similarities to Greenhills, but are interpreted to have been emplaced at very deep levels of predominantly mature island arcs (DeBari and Coleman 1989; Khan et al. 1993).

We suggest that the Greenhills Complex represents the crystallised product of relatively shallow-level, low-K tholeiitic magma reservoirs which supplied a primitive island-arc volcano. The crust is expected to have been relatively thin with elevated geothermal gradients, allowing the primitive parent magmas to ascend to high levels without significant differentiation. Magma stratification is expected to have occurred after ponding of melt in the chambers. Therefore, periodic recharging of these chambers by primitive melt most probably coincided with expulsion of residual melts and their eruption to form volcanic rocks at, or near, the surface. Recharge, venting and associated seismic activity would have caused turbulent magmatic conditions resulting in thermal erosion, dislocation of cumulates and episodic convection within the magma chambers. We expect similar processes to occur in magma reservoirs which feed modern island-arc volcanoes. The overall lack of exposures of cumulate bodies similar to the Greenhills Complex may be due to delamination and recycling of dense cumulates into the mantle wedge (Arculus 1999) or dismemberment of these bodies during evolution or accretion of the arc system.

Conclusions

The Greenhills Complex consists of two, small layered intrusions which formed as feeder reservoirs to an immature island-arc volcano. From the mineralogy and geochemistry of rocks of the Complex, we have determined the initial parent magmas to have been hydrous, low-K tholeiites of ankaramitic affinities which were produced by melting of a very primitive, clinopyroxene-rich source. Differentiation of the parent magma produced a layered series consisting of dunite, olivine clinopyroxenite, olivine gabbro and hornblende gabbro-norite. This sequence of cumulate-rock types is distinctively arc-like, reflecting the late (relative to MORB or IOB) appearance of plagioclase in the crystallisation sequence of comparably hydrous mafic magma. Evolved melts were of HAB composition and are now only preserved as dykes which cut the Layered Group. Mineralogical profiles and outcrop features indicate that turbulent magmatic conditions, magma stratification and episodic magma recharge occurred while the Complex was forming. Magma recharge was probably coincident with the expulsion and eruption of residual melt. Geochemical similarities between the evolved melt samples from Greenhills and volcanic rocks from neighbouring regions indicate that the aforementioned processes of magmatic differentiation were not restricted to the Greenhills Complex, but operated throughout this ancient island-arc terrane and may commonly take place in modern island-arc systems.

Acknowledgements This research was supported by the Australian Research Council and the ANU. Critical reviews by Susan Debari, Tom Sisson and John Gamble were most helpful and have greatly improved the manuscript.

References

Arculus RJ (1999) Origins of the continental crust. J Proc R Soc NSW 132:83–110

Arculus RJ, Powell R (1986) Source component mixing in the regions of arc magma generation. J Geophys Res 91(B):5913–5926

Arculus RJ, Wills KJA (1980) The petrology of plutonic blocks and inclusions from the Lesser Antilles island arc. J Petrol 21:743–799

Barsdell M, Berry RF (1990) Origin and evolution of primitive island-arc ankaramites from Western Epi, Vanuatu. J Petrol 31:747–777

Beard JS (1986) Characteristic mineralogy of arc-related cumulate gabbros: implication for the tectonic setting of gabbroic plutons and for andesite genesis. Geology 14:848–851

Bradshaw JD (1994) Brook Street and Murihiku terranes of New Zealand in the context of a mobile South Pacific Gondwana margin. J S Am Earth Sci 7:325–332

Brophy JG, Marsh BD (1986) On the origin of high-alumina arc basalts and the mechanics of melt extraction. J Petrol 27:763–789

Burns LE (1985) The Border Ranges ultramafic and mafic complex, south-central Alaska: cumulate fractionates of island-arc volcanics. Can J Earth Sci 22:1020–1038

Challis GA, Lauder WR (1977) The pre-Tertiary geology of the Longwood Range. N Z Geol Surv Misc Ser map 11 explanatory notes

Clemens-Knott D, Saleeby JB (1999) Impinging ring dike complexes in the Sierra Nevada batholith, California: roots of the early Cretaceous volcanic arc. Geol Soc Am Bull 111:484–496

Coleman RG, Keith TE (1971) A chemical study of serpentinisation – Burro Mountain, California. J Petrol 12:311–328

Coombs DS, Landis CA, Norris RJ, Sinton JM, Borns DJ, Craw D (1976) The Dun Mountain Ophiolite Belt, New Zealand, its tectonic setting, constitution, and origin, with special reference to the southern portion. Am J Sci 276:561–603

Cowden A, Ruddock R, Reay A, Nicolson P, Waterman P, Banks MJ (1990) Platinum mineralisation potential of the Longwood Igneous Complex, New Zealand. Mineral Petrol 42:181–195

Crawford AJ, Falloon TJ, Eggins SM (1987) The origin of island arc high-alumina basalts. Contrib Mineral Petrol 97:417–430

DeBari SM, Coleman RG (1989) Examination of the deep levels of an island arc: evidence from the Tonsina Ultramafic-Mafic Assemblage, Tonsina, Alaska. J Geophys Res 94(B):4373–4391

Della-Pasqua FN, Varne R (1997) Primitive ankaramitic magmas in volcanic arcs: a melt-inclusion approach. Can Mineral 35:291–312

Eggins SM (1993) Origin and differentiation of picritic arc magmas, Ambae (Aoba), Vanuatu. Contrib Mineral Petrol 114:79–100

Eggins SM, Rudnick RL, McDonough WF (1998) The composition of peridotites and their minerals: a laser-ablation ICP-MS study. Earth Planet Sci Lett 154:53–71

Findlay DC (1969) Origin of the Tulameen ultramafic-gabbro complex, southern British Columbia. Can J Earth Sci 6:399–425

Frost CD, Coombs DS (1989) Nd isotope character of New Zealand sediment: implications for terrane concepts and crustal evolution. Am J Sci 289:744–770

Ghiorso MS, Sack RO (1995) Chemical mass transfer in magmatic processes. IV. A revised and internally consistent thermodynamic model for the interpolation and extrapolation of liquid-solid equilibria in magmatic systems at elevated temperatures and pressures. Contrib Mineral Petrol 119:197–212

Green TH (1994) Experimental studies of trace-element partitioning applicable to igneous petrogenesis – Sedona 16 years later. Chem Geol 117:1–36

Green DH, Lus W (2000) Phase relations and magmatism in the mantle wedge above subduction zones. Goldschmidt 2000, J Conf Abstr 5(2):454

Hawkesworth CJ, Gallagher K, Hergt JM, McDermott F (1993) Mantle and slab contributions in arc magmas Ann Rev Earth Planet Sci 21:175–204

Himmelberg GR, Loney RA (1995) Characteristics and petrogenesis of Alaskan-type ultramafic-mafic intrusions, southeastern Alaska. US Geol Surv Prof Pap 1564

Houghton BF (1981) Lithostratigraphy of the Takitimu Group, central Takitimu Mountains, western Southland, New Zealand. N Z J Geol Geophys 24:333–348

Houghton BF, Landis CA (1989) Sedimentation and volcanism in a Permian arc-related basin, southern New Zealand. Bull Volcanol 51:433–450

Hunter RH (1996) Texture development in cumulate rocks. In: Cawthorn RG (ed) Layered intrusions. Elsevier Science, Amsterdam, pp 77–101

Irvine TN (1974) Petrology of the Duke Island Ultramafic Complex, southeastern Alaska. Geol Soc Am Mem 138

Ito E, Harris DM, Anderson AT (1983) Alteration of oceanic crust and geologic cycling of chlorine and water. Geochim Cosmochim Acta 47:1613–1624

James OB (1971) Origin and emplacement of the ultramafic rocks of the emigrant Gap area, California. J Petrol 12:523–560

Jan MQ, Windley BF (1990) Chromian spinel-silicate chemistry in ultramafic rocks of the Jijal Complex, Northwest Pakistan. J Petrol 31:667–715

Johan Z, Ohnenstetter M, Slansky E, Barron LM, Suppel D (1989) Platinum mineralisation in the Alaskan-type intrusive complexes near Fifield, New South Wales, Australia. Part 1. Platinum-group minerals in clinopyroxenites of the Kelvin Grove Prospect, Owendale Intrusion. Mineral Petrol 40:289–309

Kepezhinskas P, Reuber I, Tanaka H, Miyashita S (1993) Zoned calc-alkaline plutons in northeastern Kamchatka, Russia: implications for crustal growth in magmatic arcs. Mineral Petrol 49:147–174

Khan MA, Jan MQ, Weaver BL (1993) Evolution of the lower arc crust in Kohistan, N. Pakistan: temoral arc magmatism through early, mature and intra-arc rift stages. In: Treloar PJ, Searle MP (eds) Himalayan tectonics. Geol Soc Lond Spec Publ 74:123–138

Kimbrough DL, Mattinson JM, Coombs DS, Landis CA, Johnston MR (1992) Uranium-Lead ages from the Dun Mountain ophiolite belt and Brook Street terrane, South Island, New Zealand. Geol Soc Am Bull 104:429–443

Lipps JH (1970) Plankton evolution. Evolution 24:1–22

Marsh BD (1988) Crystal capture, sorting, and retention in convecting magma. Geol Soc Am Bull 100:1720–1737

Marsh BD (1995) Solidification fronts and magmatic evolution. Mineral Mag 60:5–40

Mitchell MJ (1995) Alluvial platinum-group minerals in southern New Zealand. Proc Pacrim Congr 1995:337–382

Mortimer N (1995) Triassic to Early Cretaceous tectonic evolution of New Zealand terranes: a summary of recent data and an integrated model. Proc Pacrim Congr 1995:401–406

Mossman DJ (1973) Geology of the Greenhills Ultramafic Complex, Bluff Peninsula, Southland, New Zealand. Geol Soc Am Bull 84:39–62

Mossman DJ, Force LM (1969) Permian fossils from the Greenhills Group, Bluff, Southland, New Zealand. N Z J Geol Geophys 12:659–672

Mossman DJ, Coombs DS, Kawachi Y, Reay A (2000) High-Mg arc-ankaramitic dikes, Greenhills Complex, Southland, New Zealand. Can Mineral 38:191–216

Murray CG (1972) Zoned ultramafic complexes of the Alaskan-type: feeder pipes of andesitic volcanoes. Geol Soc Am Mem 132:313–335

Myers JD, Johnston AD (1996) Phase equilibria constraints on models of subduction zone magmatism. In: Bebout BE, Scholl DW, Kirby SH, Platt JP (eds) Subduction: top to bottom. American Geophysical Union, Washington, DC, pp 229–249

Ozawa K (1984) Olivine-spinel geospeedometry: analysis of the diffusion-controlled Mg-Fe^{2+} exchange. Geochim Cosmochim Acta 48:2597–2611

Panjasawatwong Y, Danyushevsky LV, Crawford AJ, Harris KL (1997) An experimental study of the effects of melt composition on plagioclase-melt equilibria at 5 and 10 kbars: implications

for the origin of magmatic high-An plagioclase. Contrib Mineral Petrol 118:420–432
Pearce JA, Peate DW (1995) Tectonic implications of the composition of volcanic arc magmas. Ann Rev Earth Planet Sci 23:251–285
Perfit MR, Gust DA, Bence AE, Arculus RJ, Taylor SR (1980) Chemical characteristics of island-arc basalts: implications for mantle sources. Chem Geol 30:227–256
Rollinson H (1993) Using geochemical data: evaluation, presentation, interpretation. Longman, London
Schiano P, Eiler JM, Hutcheon ID, Stopler EM (2000) Primitive CaO-rich, silica-undersaturated melts in island arcs: evidence for the involvement of clinopyroxene-rich lithologies in the petrogenesis of arc magmas. Geochem Geophys Geosys 1 DOI 1999GC000032
Sisson TW, Bronto S (1998) Evidence for pressure-release melting beneath magmatic arcs from basalts at Galunggung, Indonesia. Nature 391:883–886
Sisson TW, Grove TL (1993) Experimental investigations of the role of H_20 in calc-alkaline differentiation and subduction zone magmatism. Contrib Mineral Petrol 113:143–166
Sisson TW, Grove TL, Coleman DS (1996) Hornblende gabbro sill complex at Onion Valley, California, and a mixing origin for the Sierra Nevada batholith. Contrib Mineral Petrol 126:181–108
Sivell W, Rankin P (1983) Arc-tholeiite and ultramafic cumulates, Brook Street Volcanics, west D'Urville Island, New Zealand. N Z J Geol Geophys 26:239–257
Snoke AW, Sharp WD, Wright JE, Saleeby JB (1982) Significance of mid-Mezosoic peridotitic to dioritic intrusive complexes, Klamath Mountains – western Sierra Nevada, California. Geology 10:160–166
Spandler CJ, Eggins SM, Arculus RJ, Mavrogenes JA (2000) Using melt inclusions to determine parent-magma compositions of layered intrusions: application to the Greenhills Complex (New Zealand), a platinum-group-minerals-bearing, island-arc intrusion. Geology 28:991–994
Staudigel H, Plank T, White B, Schmincke H-U (1996) Geochemical fluxes during seafloor alteration of the basaltic upper oceanic crust: DSDP sites 417 and 418. In: Bebout BE, Scholl DW, Kirby SH, Platt JP (eds) Subduction: top to bottom. American Geophysical Union, Washington, DC, pp 19–37
Sun SS, McDonough WF (1989) Chemical and isotopic systematics of oceanic basalts: implications for mantle composition and processes. In: Saunders AD, Norry MJ (eds) Magmatism in oceanic basins. Geol Soc Lond Spec Publ 42:313–345
Taylor SR, McLennan SM (1981) The continental crust: its composition and evolution. Blackwell, Oxford
Tistl M, Burgath KP, Hohndorf A, Kreuzer H, Munoz R, Salinas R (1994) Origin and emplacement of Tertiary ultramafic complexes in northwest Columbia: evidence from geochemistry and K-Ar, Sm-Nd and Rb-Sr isotopes. Earth Planet Sci Lett 126:41–59